RSC Advances

ROYAL SOCIETY OF CHEMISTRY

www.rsc.org/advances

Photoassisted hetero-Fenton degradation mechanism of Acid Blue 74 by γ-Fe_2O_3 catalyst

Shanshan Cao[1], Feifei Kang[1], Ping Li[1,2], Rufen Chen[1,2], Hui Liu[1,2,*], Yu Wei[1,2,*]

[1]College of Chemistry and Material Science, Hebei Normal University, Shijiazhuang, 050024, China

[2]Key Laboratory of Inorganic Nanomaterial of Hebei Province, Shijiazhuang, 050024, China

Email address: liuhuicn@126.com, weiyu@mail.hebtu.edu.cn

* Corresponding author

Telephone number: +86-311-80787433

Abstract:

Fusiform-like maghemite particles were prepared through a distinct two-step transformation from Fe(II) to γ-FeOOH and then to γ-Fe_2O_3 by precipitation and calcination respectively. The structure and property of as-prepared sample were characterized by XRD, SEM, XPS, UV–vis and FTIR. The degradation of Acid Blue 74 by γ-Fe_2O_3 was investigated under visible light irradiation. ^{1}H NMR, TOC, UV–VIS, direct infusion-ESI-(-)MS and FTIR spectroscopic techniques provide an insight into the nature of the degradation products. A more complete degradation mechanism of Acid Blue 74 on γ-Fe_2O_3 was presented. The results indicate the total degradation rate is close to 100% for a 100 mg/L Acid Blue 74 solution. Among them, about 60% was completely mineralized and the other 40% was degraded to aliphatic acids. The magnetic γ-Fe_2O_3 could be conveniently recovered by applying a magnet and recycled. The γ-Fe_2O_3 retained 100% degradation capacity for Acid Blue 74 after 6 cycles.

Keywords: maghemite; degradation mechanism; acid blue 74; regeneration

1. Introduction

In recent decades, various environmental challenges have been mitigated due to a boom in nanotechnologies and nanomaterials development. Some nano-sized metal oxides such as TiO_2, ZnO, CdO and various iron oxides *etc.* have been reported to be shown promising performance in pollutant removal or toxicity mitigation.[1-3] Among them, TiO_2 and iron oxides are two excellent examples. TiO_2 is widely studied due to its excellent optical and electronic properties, low cost, and photochemical stability. However, TiO_2 can only be excited by UV light (λ< 380nm) because of its wide band gap (Eg=3.2 eV).[4] To overcome this disadvantage, the modification of TiO_2 including nonmetal/metal doping, coupling with other semiconductor, *etc.* has been attempted.[5-10] However, little progress has been made in industrial application because the photocatalytic activity of modified TiO_2 is still very low under visible light radiation.[11] Various iron oxides are used in the remediation of wastewater due to the efficient and economical photo-Fenton reaction system.[12] Nonetheless, as for small sized nanoparticles, how to effectively separate the used photocatalysts restricts the industrial application of these materials.[13,14] For example, centrifugation and filtration always lead to serious catalyst loss as well as high energy consumption. In this context, magnetic nanoparticles, mainly nano zero-valent iron (nZVI), magnetite (Fe_3O_4) and maghemite (γ-Fe_2O_3) nanoparticles, have sparked an immense interest in research for treatment of polluted water.[15-18] Heavy metals such as arsenic and chromium, and organic pollutants like chlorinated solvents, can be immobilized or reduced to less toxic species by nZVI.[1] A number of studies have also shown the application of Fe_3O_4 and γ-Fe_2O_3 nanoparticles on heavy metals and organic pollutants removal from contaminated water.[19,20] Asuha et al[21] prepared the mesoporous maghemite by the thermal decomposition of $[Fe(CON_2H_4)_6](NO_3)_3$ with the aid of cetyltrimethyl ammonium bromide (CTAB), and it showed a great adsorption ability for methyl orange (MO) from wastewater. Li et al[22] synthesized magnetic γ-Fe_2O_3 nanoparticle by a co-precipitation method and found that the γ-Fe_2O_3 showed excellent adsorption capacity for both arsenite and arsenate. The magnetism of these materials is a very useful property for wastewater treatment systems. Separation of magnetic nanoparticles from solution with a low-gradient magnetic field or a hand-held magnet has been reported.[23,24] Li et al[22] found the saturated magnetic γ-Fe_2O_3 nanoparticles could be

recovered by applying a magnetic field of strength greater than 0.35 T. Arsenic compounds were eluted from the magnetic adsorbent following treatment with 1M NaOH, leading to regeneration of the magnetic γ-Fe_2O_3 nanoparticles and the nanoparticles retained over 40% of their initial adsorption capacity for arsenic compounds after 6 cycles. Though γ-Fe_2O_3 nanoparticles have shown a high reactivity in treatment of polluted water, the application of γ-Fe_2O_3 nanoparticles usually focuses on its adsorption for heavy metals and organic pollutants, few work evaluates its photocatalytic degradation ability as well as the degradation mechanism of organic pollutants.[25-27]

In this work, fusiform-like γ-Fe_2O_3 particles were prepared by a distinct two-step transformation. The catalytic activity of γ-Fe_2O_3 was studied by using Acid Blue 74 (AB 74) as a model pollutant, and the degradation products were checked by ^{1}H NMR, FTIR and direct infusion-ESI-(-)MS. The possible degradation mechanism of AB 74 and the recovery and regeneration of γ-Fe_2O_3 were investigated.

2. Experimental

2.1. Materials

The ferric sulfate ($FeSO_4 \cdot 7H_2O$) and ethylene diamine tetraacetic acid (EDTA) and ammonium hydroxide (NH_4OH) were analytical grade, and used without further purification. 5,5'-Indigotindisulfonic acid disodium salt ($C_{16}H_8N_2Na_2O_8S_2$) named commercially Acid Blue 74 (AB 74) was purchased from J&K. The structure of AB 74 is shown in Fig. S1.

Fig. S1.

2.2. Synthesis

Precursor γ-FeOOH was firstly synthesized according to the following procedures.[28] 10 mL of EDTA (0.015 mol/L) and 110 mL of $FeSO_4$ (0.3 mol/L) were mixed in a 250 mL flask. 8 mL concentrated NH_4OH solution was used to adjust the pH to 8.6 and the total volume of the solution was adjusted to 150 mL with distilled water. Air was then passed at a rate of 0.272 m^3/h through the pump. The change in pH during oxidation was monitored using a digital pH meter. When the pH of the system reaches 4.3, the preparation reaction of γ-FeOOH was completed. The precipitate was collected by filtrating and was washed. The above process was carried out under vigorous stirring at room temperature. The

powder was dried at about 50 °C for 24 h. Based on the transformation temperature obtained by TG-DSC (258.16 °C), the γ-FeOOH powder was heated at 260 °C for 2 h to prepare γ-Fe_2O_3.

2.3. Characterization

X-ray diffraction (XRD) measurement was carried out at room temperature using a D8ADVANCE diffractometer with CuKα radiation (λ=0.15418 nm). Scanning electron microscopy (SEM) images were taken with an S-4800 scanning electron microscope (Japan Hitachi LTD). X-ray photoelectron spectroscopy (XPS) data were acquired by using a PHI-5000 Versa Probe. Fourier transform infrared spectra (FTIR) of the samples were recorded with FTIR-8900 spectrometer (Japan Hitachi LTD) at room temperature. UV-vis diffuse reflectance spectra of the as-obtained samples were recorded by using a U-3010 UV-vis spectrophotometer(Japan Hitachi LTD).^{1}H NMR spectra were recorded on a AV Ⅲ-300 BRUKER spectrometer. The electrospray ionization mass spectrometry (ESI) were obtained with a AB SCIEX 3200Q-TRAP mass analyzer at a typical ESI conditions. Total organic carbon (TOC) was analyzed with a lquiTOC□analyzer (Elementar Analytik, Germany).

2.4. photocatalytic degradation experiments

All experiments were conducted in a 250 mL photoreactor. The temperature inside the reactor was kept constant (20 °C) by circulating water within the jacket surrounding the reactor. The visible-light irradiation was provided by a 10 W lamp (λ > 400 nm, Fhilips, China). The distance between the light source and the solution is 60 cm.

Photocatalytic degradation of AB 74 was carried out in a cylindrical water-jacketed glass reactor using a constant solution volume of 150 mL. The initial concentration of AB 74 is 100 mg/L and the initial pH is 4. The dosage of catalyst is 0.6 g/L. The temperature of the solution was maintained constant at 20 °C with circulating water. During irradiation, the solution was stirred in a constant rate. The concentrations of AB 74 in the solution before and during the degradation were determined using a UV–vis spectrophotometer at 610 nm. For studying the effect of pH on dye degradation, the pH of the dye solution was adjusted by adding dilute H_2SO_4 or NaOH solutions.

2.5 H_2O_2 decomposition experiments

Evaluation of catalytic activity of γ-Fe_2O_3 in the decomposition of hydrogen peroxide

was carried out according to the method described in Ref.[29]. Briefly, the experiments were conducted in a batch reactor using a constant solution volume of 250 mL that was stirred at a speed to provide complete mixing for uniform distribution and full suspension of γ-Fe_2O_3 particles. 0.15 g of γ-Fe_2O_3 was respectively added into the systems. The pH was adjusted by using NaOH or H_2SO_4 solutions. The samples taken at one hour intervals were filtered to separate the iron oxide particles from the solution. The concentration of H_2O_2 in filtrate was measured according to the permanganate titration method that has a detection limit of 1×10^{-4} M of H_2O_2.[29]

3. Results and discussion

3.1. Characterization of samples

To determine the transformation temperature of γ-FeOOH, the TG-DSC curves are shown in Fig. 1. As can be seen in Fig. 1a, γ-FeOOH has two weight loss steps from 0 to 450 °C. The drop of 4.9 % below 100 °C results from the removal of absorbed water, and the second one of 9.9 % from 100 to 450 °C is assigned to the transformation from γ-FeOOH to γ-Fe_2O_3, which is corresponding to the phase inversion temperature (258.16 °C) of γ-FeOOH. Based on the data in Fig. 1a, γ-FeOOH was annealed at 260, 320 and 400 °C, respectively. The XRD patterns (Fig. S2) indicate that the three samples are pure phase γ-FeOOH. Figs. 1b and 1c present the XRD and XPS patterns of the precursor γ-FeOOH and its transformation product annealed at 260 °C. The diffraction peaks of γ-FeOOH could be well indexed to JCPDS card No. 00-074-1877. In the XRD pattern of the transformation product of γ-FeOOH, six diffraction peaks appeared at 2θ 30.30, 35.68, 43.40, 54.20, 57.32 and 62.96°, correspond to γ-Fe_2O_3 (JCPDS Card No. 00-039-1346). No other peaks were observed, indicating that γ-FeOOH had been completely converted into γ-Fe_2O_3. In Fig. 2c, the electron-binding energy of Fe2p 3/2 and Fe2p 1/2 are, respectively, 711.2 and 725.0 eV for γ-FeOOH and 710.8 and 724.4 eV for γ-Fe_2O_3, with a split of 13.8 and 13.6 eV between the two peaks, which is identical to the reported results.[30,31] In the corresponding IR spectra shown in Fig. S3, the bands at 1022 and 748 cm^{-1} are characteristic peaks of γ-FeOOH, while the two bands disappear in the sample of γ-Fe_2O_3. The bands at 556 and 444 cm^{-1} are attributed to the Fe–O stretching of γ-Fe_2O_3.[32] The results above also indicate that γ-FeOOH has converted to γ-Fe_2O_3. The broad band at ~3436 cm^{-1} is ascribed to OH stretching vibrations, and bands

at ~1644 cm^{-1} can be ascribed to the OH bending vibrations. Theoretically, there is no –OH groups in maghemite structure. However, some defects such as Fe^{3+} cation vacancy sites easily formed in the process of crystal growth, especially near the surface of crystal particles. One vacant Fe^{3+} cation site is charge compensated by the presence of three protons, forming hydroxyls with the O atoms surrounding the vacant cation site. Experimental evidence suggests that these excess –OH groups on vacant cation sites in maghemite can be identified by characteristic FTIR modes.[33]

Fig. 1.

Fig. 2.

Fig. 2 shows the SEM images of lepidocrocite (a) and maghemite (b). As can be seen in Fig. 2, both lepidocrocite and maghemite composed of many uniform fusiform-like particles with diameters of about 500 nm and length of about 0.8 μm. Lepidocrocite and maghemite are similar in morphology and crystallite size.

Fig.3.

The magnetic properties of the synthesized γ-Fe_2O_3 were studied by using a Physical Properties Measurement System at room temperature. From the magnetization curves shown in Fig. 3, it was known that the saturation magnetization (Ms) and coercivity (Hc) of the sample are 36.8 emu/g and 90.8 Oe, respectively, suggesting that as-prepared γ-Fe_2O_3 is ferromagnetic at room temperature. This is useful for water and wastewater treatment systems. It is expected that magnetic separation could be a more cost effective and convenient method for separating such tiny particles than sophisticated membrane filtration.

Fig. 4a shows the UV-vis spectra of sample γ-Fe_2O_3. These powders have an obvious absorption edge at about 618 nm in the visible light region. The band gap energy Eg of the sample can be more accurate calculated by using equation (1):

$$ah\nu = A(h\nu - Eg)^{n/2} \quad (1)$$

where a, h, ν, A, and Eg are the absorption coefficient, Planck constant, light frequency, a

constant, and band gap, respectively. Thereinto, n depends on the characteristics of the transition in a semiconductor, which is either 1 for direct interband transition or 4 for indirect inter-band transition.[11] For γ-Fe_2O_3, the value of n is 1 for the direct transition. Fig. 4b shows the $(ahv)^2$ vs photon energy *hv* curve for the γ-Fe_2O_3. The Eg values of as-synthesized γ-Fe_2O_3 sample is estimated to be 2.0 eV from the $(ahv)^2$ - *hv* plots, which is consistent with the red color observed for γ-Fe_2O_3 powders.

Fig. 4

3.2. Selection of conditions for photocatalytic degradation of AB 74 on γ-Fe_2O_3

Prior to the photocatalytic reaction, the suspension was stirred in the dark. The adsorption capacity of AB 74 on γ-Fe_2O_3 (obtained at 260 °C) changes with time was determined (Fig. S4). The result shows that AB 74 needs about 40 min to establish an adsorption/desorption equilibrium. The maximum adsorption capacity is ca. 54.54 mg/g. To investigate the catalytic action of γ-Fe_2O_3 on the degradation of AB 74, five control experiments were designed. The first one was a blank experiment without γ-Fe_2O_3 under visible light (Fig. 5a). The result shows that the concentration of AB 74 didn't change with time, suggest AB 74 in solution is stable during the study period (9 h). In the second control experiment, 0.6 g/L of γ-Fe_2O_3 was added into the reaction system. The result shows that the concentration of AB 74 didn't change with time (Fig. 5b). In the third control experiment, 0.01 mol/L H_2O_2 was added into the reaction system based on the first control experiment. No obvious degradation of AB 74 was observed over 9 h of irradiation, which meant that the combination of visible light and H_2O_2 was ineffective (Fig. 5c). In the fourth control experiment, 0.6 g/L of γ-Fe_2O_3 and 0.01 mol/L of H_2O_2 were added into the reaction system and the reaction was conducted in the dark. It was found that about 80% of AB 74 was degraded (Fig. 5d). In the fifth control experiment, when γ-Fe_2O_3, H_2O_2 and irradiation of visible light were introduced into the reaction system, about 95% of AB 74 was degraded (Fig. 5e). These results indicate that, on the one hand, the coexistence of γ-Fe_2O_3 and H_2O_2 could accelerate obviously the degradation of AB 74 and on the other hand, the combination of γ-Fe_2O_3, H_2O_2 and visible light provide the most effective conditions for the degradation of AB 74. The result in Fig. 4 indicates that the Eg values of γ-Fe_2O_3 sample is about 2.0 eV, suggesting

that it is favorable for γ-Fe_2O_3 adsorbing visible light. Therefore, this reaction system was chosen for investigation in the present paper. It was reported that iron oxides can catalyze the decomposition of hydrogen peroxide to produce hydroxyl radicals (·OH), which can oxidize most of organic substances, owing to their high oxidation potential (E^0 = 2.80V).[34] The current results indicate that the visible light irradiation further accelerates this process. A little Eg value (2.0 eV) for γ-Fe_2O_3 is favorable for its absorption for the visible light.

Fig. 5.

Subsequently, the degradation of AB 74 was studied using the three γ-Fe_2O_3 samples obtained at different temperatures as catalysts. It was found that there is no obvious difference between them (Fig. S5). Therefore, the γ-Fe_2O_3 prepared at 260 °C was selected as candidate in the subsequent experiments.

Moreover, the degradation of AB 74 with initial concentration varying from 60 to 120 mg/L was investigated. The pH of the reaction system was adjusted to 4.0. The changes of degradation capacity of AB 74 with time under different initial concentrations are shown in Fig. S6. As can be seen in Fig. S6, γ-Fe_2O_3 exhibits the excellent catalytic degradation ability. When the initial concentration of AB 74 is 60 mg/L, 100% of dye was degraded within 3 h. With increasing the concentration of dye, the time completed degradation prolonged. When the initial concentrations of AB 74 are 100 and 120 mg/L, the degraded capacity of AB 74 reached about 98 and 112 mg/L, respectively. The initial concentration of AB 74 in the following reaction system was selected as 100 mg/L.

Actually, the catalyst dosage has a certain influence on the photocatalytic degradation of dye.[35,36] Fig. 6 presents the degradation rate of AB 74 at different catalyst dosage with time. The initial reaction rates were found to increase with an increase in the amount of catalyst, reached the higher value (0.80 g/L of the catalyst). The increase of initial reaction rates may probably be due to: (i) increase in the adsorption capacity of dye molecules on γ-Fe_2O_3 surface; (ii) increase in the number of surface active sites of γ-Fe_2O_3; (iii) increase in the decomposition rate of H_2O_2. However, when the catalyst dosage increases from 0.60 to 0.80 g/L, only a little increase of reaction rate was detected which may be attributed to (i) the agglomeration of γ-Fe_2O_3 particles at higher loading

which covers the part of photosensitive area retarding both photon and dye absorption; (ii) turbidity at higher γ-Fe_2O_3 loading results in the shadowing effect thus decreasing the penetration depth of light irradiation; (iii) high degree of scattering by γ-Fe_2O_3.[37] Based on the results above, the catalyst dosage in the current system was selected as 0.60 g/L .

Fig. 6.

3.3 Effect of pH on the degradation of AB 74

The changes of the degradation rate with time at different pHs for AB 74 solution of 100 mg/L were determined and the results are shown in Fig. 7. The degradation rate of AB 74 was strongly pH dependent. The degradation rates of AB 74 decreased from pH 3 to 7 and increased slightly in the pH range of 7–10. However, a higher degradation rate is observed at pH 11. A similar result has been reported by Houria et al.[37] We speculate that there are two factors to influence the degradation rate of AB 74. One is the catalytic decomposition rate of H_2O_2 and the other is the adsorption capacity of AB 74, both of which vary with pHs. For this reason, the adsorption capacity of AB 74 on γ-Fe_2O_3, the catalytic decomposition rates of H_2O_2 at different pHs and the point of zero charge pzc of γ-Fe_2O_3 were determined and the results are also shown in Fig. 7. As can be seen in Fig. 7b, the adsorption capacity of AB 74 decreases with increasing pH. From Fig. S1, it was known that AB 74 has a sulphuric group in its structure, suggesting that AB 74 molecular usually exists in solution in the form of anions. Fig. 7c indicates that the pzc of γ-Fe_2O_3 is about 6.3. Thus, when pH < pH_{pzc}, the surface of γ-Fe_2O_3 is positively charged, which is favorable for the adsorption of AB 74. It was noted that both the adsorption capacity of AB 74 and the decomposition rate of H_2O_2 at pH 4 are larger than those at pH 7. The two factors result in a higher degradation rate of AB 74 at pH 4. However, Fig. 7b indicates that the adsorption capacity of AB 74 is little at pH 11, while its degradation rate is closed to 100% (Fig. 7a). To understand this result, we also determined the decomposition rate of H_2O_2 at different pHs only under visible light irradiation without γ-Fe_2O_3. Fig. 7d reveals that H_2O_2 can be decomposed only under visible light irradiation at pH 11 while the similar phenomenon wasn't observed both at pH 4 and 7. The conjugate base of H_2O_2 increases at alkaline pH and HO_2^- has a higher cross-section, which favors the absorption of light and should normally increase the •OH (Eqs.

(2)–(4))[38,39]

$$H_2O_2 \rightarrow HO_2^- + H^+ \quad (2)$$

$$HO_2^- + H^+ + h\nu \rightarrow 2\ \bullet OH \quad (3)$$

$$\bullet OH + RH \rightarrow R\bullet + H_2O \quad (4)$$

In addition, the catalytic decomposition rate of H_2O_2 by γ-Fe_2O_3 at pH 11 is also larger than that at other pHs (Fig. 7d). Thus, the total decomposition rate of H_2O_2 is the largest among the three systems (pH= 4, 7 and 11). Though the adsorption capacity of AB 74 isn't large at pH 11, a rapid decomposition of H_2O_2 results in more production of •OH and then a high degradation rate of AB 74.

Fig. 7.

3.4. Degradation mechanism of AB 74

To further reveal the degradation mechanism of AB 74 on γ-Fe_2O_3, the by-products formed after the degradation of AB 74 are monitored by different techniques. The digital photos and UV-Vis spectra during the degradation process of AB 74 are displayed in Fig. 8. Before degradation, the color of AB 74 is dark blue (Fig. 8). At this time, AB 74 shows that the maximum absorption band is at ~610 and ~298 nm, respectively. With time, the color of the system becomes light and the two absorption peaks weakened. For example, the system exhibits a light-blue color at 5 h and a light-yellow color at 6 h and completely discolors at 10 h. The peak at 610 nm almost disappears after 6 h, while the peak at 298 nm doesn't completely disappear, and new absorption bands appear in ultraviolet regions. This result implies that the structure of AB 74 has been destroyed due to the powerful oxidation ability of γ-Fe_2O_3/H_2O_2/visible light. According to the data obtained at 610 nm, the degradation rate reaches to 98.5% at 6 h and 99.3% at 10 h. To evaluate whether AB 74 simply lost its color or not, a total organic carbon (TOC) analysis was performed. TOC values reflect the amount of organics in the solution, and therefore, the changes in TOC mirror the degree of degradation of an organic substrate. The result indicated that the TOC is reduced by 60% for a 100 mg/L solution of AB 74, suggesting that 40 % of AB 74 were oxidized to other small molecule products.

Fig. 8.

Subsequently, the degradation products were examined by ^{1}H NMR spectroscopy.

The resulting spectra, presented in Fig. 9a, were recorded after various irradiation times (0, 6 and 10 hours). For the sample of 0 h, which corresponds to a dark-blue solution, the signals situated at 6.6, 7.6 and 7.9 ppm are the fingerprint of AB 74.[40] For the sample of 6 h, which corresponds to a yellow solution, disappearance of signals situated at 6.6, 7.6 and 7.9 ppm, indicates the complete elimination of the original dye. However, AB 74 is not fully mineralized, since some peaks between 9 and 7 ppm are still detected. The presence of such signals is a proof of a non-destructive modification of the aromatic rings. It is worth noting that multiplets at 7.0, 7.7 and 7.8 ppm actually correspond to isatinsulfonic acid, suggesting that isatinsulfonic acid is the primary stable breakdown product during the oxidation of AB 74. Consequently, the C=C double bond in AB 74 is the most vulnerable part of the molecule toward •OH-induced oxidation and AB 74 is converted into derivatives which carry deshielded protons (7–9 ppm), i.e. aromatic compounds. In the ^{1}H NMR spectroscopy of the colorless intermediates (the sample of 10 h), these signals are no longer detected indicating that the isatinsulfonic acid was completely consumed. A thin singlet detected at 8.2 ppm corresponds to a very deshielded proton. We are inclined to consider it to be due to formic acid.[41]

Electrospray ionization mass spectrometry in the negative ion mode, ESI(-)-MS, was used to characterize the by-products formed after the degradation of AB 74. The obtained results and the structural formulas of the products are also shown in Fig. 9b and c. In Fig. 9b, for pure AB 74 (the sample of 0 h), the presence of the anion of m/z 421 was detected (the deprotonated form of AB 74). For the sample obtained at 6 h, this anion is no longer detected indicating that the dye was completely consumed, while other anions of m/z 226 the most abundant, 244, and 216 can be observed. Product B, with a nominal mass of 227 Da, detected in its deprotonated form ([Product B-H]$^{-}$ of m/z 226), is likely to be formed via the oxidation of AB 74. This oxidation process essentially comprises the insertion of oxygen atoms at the C2 and C2′ of structure A, which probably occurs at the composite surface.[42] The formation of structure B, which does not have a conjugated system analogous to A, could well explain the discoloration of the solution, as observed. The formation of other products (C and D) from compound B could easily be explained by taking into account some simple and logical reaction pathways, as shown in Fig. 9c. Such products were detected as [C-H]$^{-}$, of m/z 244, and [D-H]$^{-}$, of m/z 216, as shown in Fig. 9b.

In the sample obtained at 10 h in Fig. 9b, the yellow intermediates anion is no longer detected indicating that the aromatic yellow intermediates were completely consumed and other multiplets relative to aliphatic intermediates are detected after a 10 h irradiation. Formic acid (m/z = 46), acetic acid (m/z = 60) and succinic acid (m/z = 118) have actually been detected after derivatization. The production of such acids is also responsible for the drop of the pH of the solution from 4.0 to 1.5 during the treatment. It is noteworthy that the degradation of AB 74 by Fenton-like leads to the formation of the same set of products as other processes encountered in the literature,[43,44] indicating a shared mechanism with the same key steps.

Fig. 9.

FTIR spectra were also used to gain information about the nature of degradation products (Fig. S7). The band intensities of the alkene bond (1613 cm^{-1}) and the aromatic moieties (C=C at 1645, and 1464 cm^{-1}) decreased with irradiation time. This is the sign of the disappearance of the original pollutant and of its primary benzenic breakdown products. Simultaneously, there is a collapse the absorbance in the range 1000–1250 cm^{-1}, which corresponds to the disappearance of stretching vibrations in sulfonate groups. Moreover, after prolonged irradiation to 10 h, the bands due to succinic acid (1685 cm^{-1}), and to an interaction between the C–O stretching and the O–H bending carboxylic acid, probably acetic acid (1416 cm^{-1}), are apparent.[45] It is noteworthy that no traces of isatinsulfonic acid could be detected by the techniques.

According the results of ^{1}H NMR, UV–VIS, FTIR, TOC and ESI(-)-MS, a more complete degradation mechanism can be presented and the results are shown in Fig. 10. Firstly, The dye AB 74 was converted to isatinsulfonic acid (structure B in Fig. 9c). This oxidation process essentially comprises the insertion of oxygen atoms at the C2 and C2′ positions of structure A due to the C=C double bond in AB 74 is the most vulnerable part of the molecule toward •OH-induced oxidation. And then, the isatinsulfonic acid was oxidized to aliphatic acid like formic acid, acetic acid and succinic acid and carbon dioxide and other small molecules. The experiments showed that benzenic compounds have been partly transformed into aliphatic acids rather than total carbon dioxide. However, this is not a real problem, since the ultimate aliphatic breakdown products are

nontoxic and biodegradable.[40] Therefore, it can be concluded that the γ-Fe_2O_3/H_2O_2 process may be, in the future, a good alternative to physical methods in use to discolor textile wastewaters.

Fig. 10.

3.5. Recovery and regeneration of γ-Fe_2O_3

γ-Fe_2O_3, as a magnetic material, is useful for water and wastewater treatment systems. It is expected that magnetic separation could be a more cost effective and convenient method for separating such tiny particles than sophisticated membrane filtration. In order to investigate the recovery efficiency of the used γ-Fe_2O_3 in water as a function of the magnetic field strength, 0.06 g/L of γ-Fe_2O_3, which had reacted with AB 74 solution with an initial concentration of 100 mg/L, pH 4.0, was separated from wastewater by the magnet at 25°C. The used magnetic γ-Fe_2O_3 nanoparticles were eluted with 0.1 mol/L aqueous HCl, 0.1 mol/L aqueous NaOH and H_2O, respectively, and then subjected to the degradation of AB 74 (100 mg/L) once more. To test the suitability and stability of the γ-Fe_2O_3, it was subjected to successive degradation cycles. The procedure was carried out 6 times and the results are shown in Fig. S8. It can clearly be seen in Fig. S8, the recovery degradation efficiency of the used γ-Fe_2O_3 were ca.100% after six regeneration in three solutions, which suggests that γ-Fe_2O_3 in this study has good reusability. The results nevertheless prove that magnetic γ-Fe_2O_3 nanoparticles can be used repeatedly in a degradation cycle. This is an essential advantage of the magnetic nanoparticles with regard to practical applications.

4. Conclusions

In summary, fusiform-like γ-Fe_2O_3 particles were successfully prepared through a distinct two-step transformation from Fe(II) to γ-FeOOH and then to γ-Fe_2O_3. The γ-Fe_2O_3 exhibits high photocatalytic activity for the degradation of dye AB 74 under visible light irradiation. For a 100 mg/L AB 74 solution, the degradation rate reaches 99.3%. 60 % of AB 74 was completely mineralized and the other 40% was oxidized to small molecule products. Based on the results obtained by ^{1}H NMR, TOC, UV-VIS, direct infusion-ESI-(-)MS and FTIR spectra, a more complete degradation mechanism of

AB 74 on γ-Fe_2O_3 was presented. The further results indicate that the as-prepared γ-Fe_2O_3 could be conveniently recovered by applying a magnet. The γ-Fe_2O_3 retained 100% degradation capacity for AB 74 after six cycles. γ-Fe_2O_3 catalyst is found to be a viable and reusable catalyst for the treatment of dye wastewater.

Acknowledgments

This work was supported by a grant from the Natural Science Foundation of China (21277040, 21477032) and Hebei Province (B2012205041, B2013205069).

References

[1] S. C. N. Tang and I. M. C. Lo, *Water Res.*, 2013, **47**, 2613–2632.

[2] L. Gomathi Devi and R. Kavitha, *RSC Adv.*, 2014, **4**, 28265-28299.

[3]S. Girish Kumar and K. S. R. Koteswara Rao, *RSC Adv.*, 2015, **5**, 3306-3351.

[4] B. Z. Tian, T. T. Wang, R. F. Dong, S. Y. Bao, F. Yang, and J. L. Zhang, *Appl. Catal. B: Environ.,* 2014, **147**, 22–28.

[5] J. C. Yu, W. K. Ho, J. G. Yu, H. Y. Yip, P. K. Wang and J. C. Zhao, *Environ. Sci. Technol.,* 2005, **39**, 1175–1179.

[6] X. Shu, Z. An, L. Wang and J. He, *Chem. Commun.,* 2009, **39**, 5901–5903.

[7] F. Chen, W. Zou, W. Qu, and J. Zhang, *Catal. Commun.,* 2009, **10**, 1510–1513.

[8] K. Nagaveni, M. S. Hegde, N. Ravishankar, G. N. Subbanna, and G. Madrad, *Langmuir*, 2004, **20**, 2900–2907.

[9] S. Girish Kumar and L. Gomathi Devi, *J. Phys. Chem. A*, 2011, **115**, 13211-13241.

[10] L. Gomathi Devi and R. Kavitha, *Appl. Catal. B: Environ.*, 2013, **140-141**, 559-587.

[11] H. Liu, W. R. Cao, Y. S, Y. W, X. H. W, *Appl. Catal. B: Environ*., 2012, **111–112**, 271–279.

[12] B. Muthukumari, K. Selvam, I. Muthuvel and M. Swaminathan, *Chem. Eng. J*., 2009, **153**, 9–15.

[13] M. M. Ye, Q. Zhang, Y. X. Hu, J. P. Ge, Z. D. Lu, L. He, Z. L. Chen and Y. D. Yin, *Chem. Eur. J*., 2010, **16**, 6243–6250.

[14] X. Guo, N. Chen, C. P. Feng, Y. N. Yang, B. G. Zhang, G. Wang, Z. Y. Zhang, *Catal. Commun*., 2013, **38**, 26–30.

[15] J. Hu, I. M. C. Lo and G. H. Chen, *Water Sci. Technol*., 2004, **50**,139–146.

[16] J. Hu, G. H. Chen and I. M. C. Lo, *Water Res*., 2005, **39**, 4528–4536.

[17] J. Hu, I. M. C. Lo and G. H. Chen, Langmuir, 2005, **21**, 11173–11179.

[18] L. Gomathi Devi, K. S. Anantha Raju and S. Girish Kumar, *J. Enviorn. Monit.*, 2009, **11**, 1397-1404.

[19] J. Hu, G. H. Chen and I. M. C. Lo, *J. Environ. Eng.*, 2006, **132**, 709–715.

[20] P. Xu, G. M. Zeng, D .L. Huang, C. L. Feng, S. Hu, M. H. Zhao, C. Lai, Z. Wei, C. Huang, G. Xin, and Z. F. Liu, *Sci. Total Environ*., 2012, **424**, 1–10.

[21] S. Asuha, Y. W. Gao, W. Deligeer, M. Yu, B. Suyala and S. Zhao, *J. Polym. Mater*.,

2011, **18**, 581–587.

[22] S. Li, D. N. Lu and Z. Liu, *Chem. Eng. J*., 2012, **211–212**, 46–52.

[23] J. Hu, I. M. C. Lo and G. H Chen, *Sep. Purif. Technol*., 2007, **56**, 249–256.

[24] W. Yantasee, C. Warner, T. Sangvanich, R. S. Addleman, T. G. Carter, R. J. Wiacek, G. E. Ryxell, C. Timchalk and M. G. Warner, *Environ. Sci. Technol*., 2007, **41**, 5114–5119.

[25] Z. W. Wei, X. C. Wei, S. Y. Wang and D. Y. He, *Mater. Lett.*, 2014, **118**, 107-110.

[26] X. X. Yu, S. W. Liu and J. G. Yu, *Appl. Catal. B: Environ.*, 2011, **104**, 12-20.

[27] S. K. Apte, S. D. Naik, R. S. Sonawane, and B. B. Kale, *J. Am. Ceram. Soc.*, 2007, **90**, 412-414.

[28] Y. L Lin, Y. Wei and Y. H Sun, *J. Mol. Catal. A: Chem*., 2012, **353–354**, 67–73.

[29] S. S. Lin and M. D. Gurol, *Environ. Sci. Technol*., 1998, **32**, 1417–1423.

[30] A. P. Grosvenor, B. A. Kobe, M. C. Biesinger and N. S. McIntyre, *Surf. Interface Anal.*, 2004, **36**, 1564–1574.

[31] T. Hyeon, S. S. Lee, J. N. Park, Y. H. Chung and H. B. Na, *J. Am. Chem. Soc*., 2001, **123**, 12798–12801.

[32] J. Lu, X. L. Jiao, D. R. Chen and W. Li, *J. Phys. Chem. C*., 2009, **113**, 4012–4017.

[33] N. Pinney and D. Morgan, *Geochim. Cosmochim. Ac*., 2013, **114**, 94–111.

[34] W. R. Haag and C. C. David, *Environ. Sci. Technol*., 1992, **26**, 1005–1013.

[35] L. Gomathi Devi and S. Girish Kumar, *Appl. Surf. Sci.*, 2012, **261**, 137-146.

[36] B. Subash, B. Krishnakumar, R. Velmurugan, M. Swaminathan and M. Shanthi, *Catal. Sci. Technol.*, 2012, **2**, 2319-2326.

[37] H. Ghodbane and O. Hamdaoui, *Chem. Eng. J*., 2010, **160**, 226–231.

[38] O. Legrini, E. Oliveros and A. M. Braun, *Chem. Rev.*, 1993, **93**, 671–698.

[39] F. J. Beltra`n, M. Gonza`lez and J. F. Gonza`lez, *Water Res*., 1997, **31**, 2405–2414.

[40] C. Galindo, P Jacques and A. Kalta, *J. Photoch. Photobio. A,*. 2001, **141**, 47–56.

[41] C. Galindo, P. Jacques and A. Kalta, *J. Photoch. Photobio. A.*, 2000, **130**, 35–47.

[42] F. V. D. Andrade, G. M. D. Lima, R. Augusti, M. G. Coelho, J. D. Ardisson, O. B. Romero and F.V.D. Andrade, *Chem. Eng. J*., 2012, **180**, 25–31.

[43] M. G. Coelho, G. M. D Lima, R. Augusti, R. D. A. Maria and J. D. Ardisson, *Appl. Catal. B: Environ*., 2010, **96**, 67–71.

[44] M. G. Coelho, G. M. D. Lima, F. V. D. Andrade, M. P. Ferreira, R. Augusti, D. A. Maria and J. D. Ardisson, *Appl. Organomet. Chem.*, 2011, **25**, 220–225.

[45] J. M. G. Amores, V. S. Escribano, R. Gianguido and G. Busca, *Appl. Catal. B: Environ*., 1997, **13**, 45–58.

Figure captions

Fig. 1. TG-DSC curves(a), XRD (b) and Fe2p XPS (c) patterns of as-prepared γ-FeOOH and γ-Fe_2O_3

Fig. 2. SEM images of the as-prepared samples. (a) γ-FeOOH; (b) γ-Fe_2O_3

Fig. 3. Magnetization curves of γ-Fe_2O_3

Fig. 4. (a) UV-vis diffuse reflectance spectra and (b) plots of $(ahv)^2$ versus photon energy hv of the γ-Fe_2O_3 samples

Fig. 5. Changes of the degradation rate of AB 74 with time under different conditions. c_{AB74} = 100 mg/L, pH=4.0, c_{H2O2}= 0.01 mol/L, The dose of γ-Fe_2O_3 is 0.6 g/L.

(a) AB 74+Visible light;

(b) AB 74+ γ-Fe_2O_3 + Visible light;

(c) AB 74+ H_2O_2 +Visible light;

(d) AB 74+ H_2O_2 + γ-Fe_2O_3;

(e) AB 74+ H_2O_2 + γ-Fe_2O_3 + Visible light

Fig. 6. Changes of the degradation rate of AB 74 at different catalyst dosage with time.

Fig. 7. (a) Changes of the degradation rate of AB 74 at different pHs with time.

(b) Changes of the adsorption capacity of AB 74 on γ-Fe_2O_3 with pH.

(c) The pH_{pzc} of γ-Fe_2O_3

(d) The catalytic decomposition of H_2O_2 at different pHs.

Fig. 8. Digital photos (a) and UV-vis absorption spectra (b) of the system at different times.

Fig. 9. (a) ^1H NMR spectra of AB 74 before irradiation and after 6 and 10 h treatment (solvent: D_2O). c_{AB74}=100 mg/L; c_{H2O2}=0.01 mol/L; natural pH; 5 ml treated.

(b) ESI(-)-MS of AB 74, samples withdrawn at 6 and 10 h.

(c) The degradation products of AB 74 in aqueous solution

Fig. 10. Proposed mechanism for the degradation of AB 74 in the present system

Figures

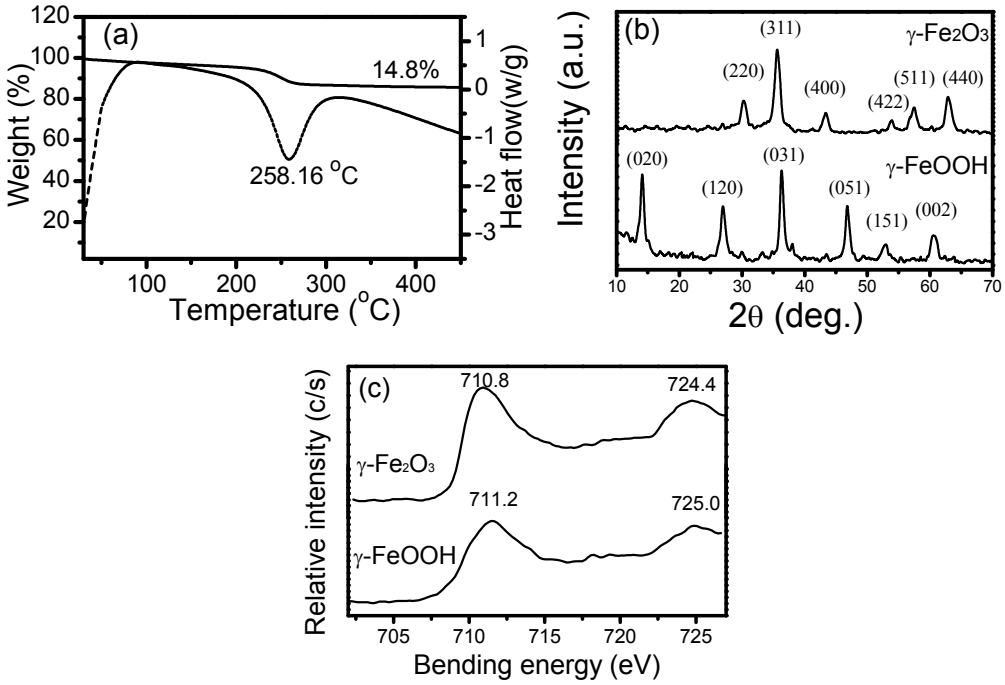

Fig. 1. TG-DSC curves(a), XRD (b) and Fe2p XPS (c) patterns of as-prepared γ-FeOOH and γ-Fe_2O_3

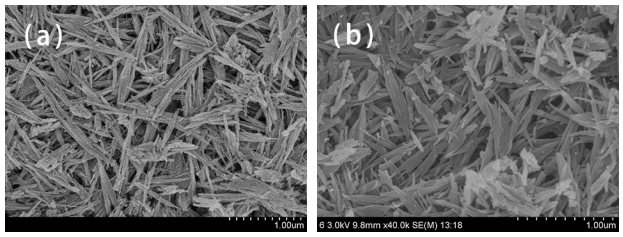

Fig. 2. SEM images of the as-prepared samples (a) γ-FeOOH; (b) γ-Fe_2O_3

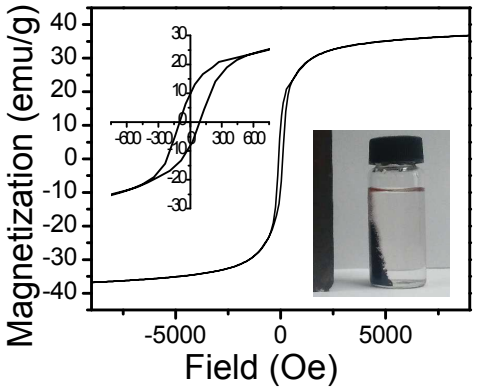

Fig.3. Magnetization curves of γ-Fe_2O_3

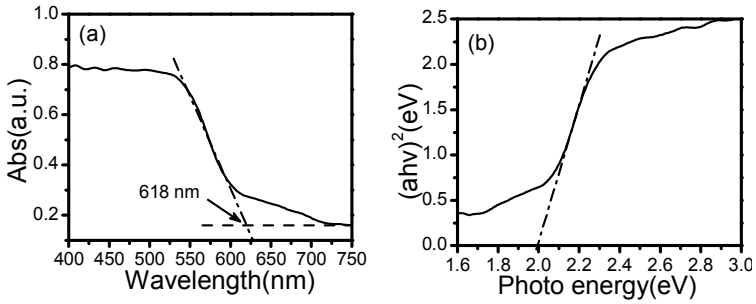

Fig. 4 (a) UV-vis diffuse reflectance spectra and (b) plots of $(ahv)^2$ versus photon energy hv of the γ-Fe_2O_3 samples

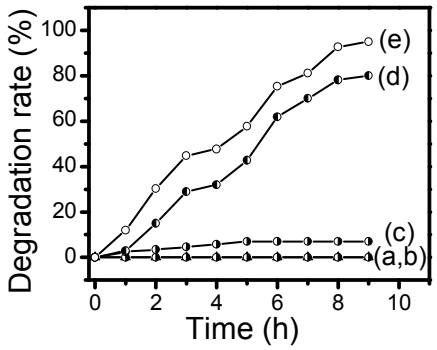

Fig. 5. Changes of the degradation rate of AB 74 with time under different conditions. c_{AB74} = 100 mg/L, pH=4.0, c_{H2O2}= 0.01 mol/L, The dose of γ-Fe_2O_3 is 0.6 g/L.
(a) AB 74+Visible light; (b) AB 74+ γ-Fe_2O_3 + Visible light; (c) AB 74+ H_2O_2 +Visible light; (d) AB 74+ H_2O_2 + γ-Fe_2O_3; (e) AB 74+ H_2O_2 + γ-Fe_2O_3 + Visible light

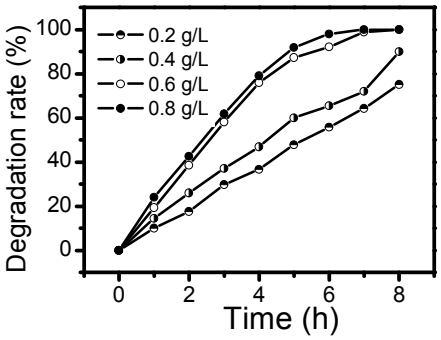

Fig. 6. Changes of the degradation rate of AB 74 at different catalyst dosage with time.

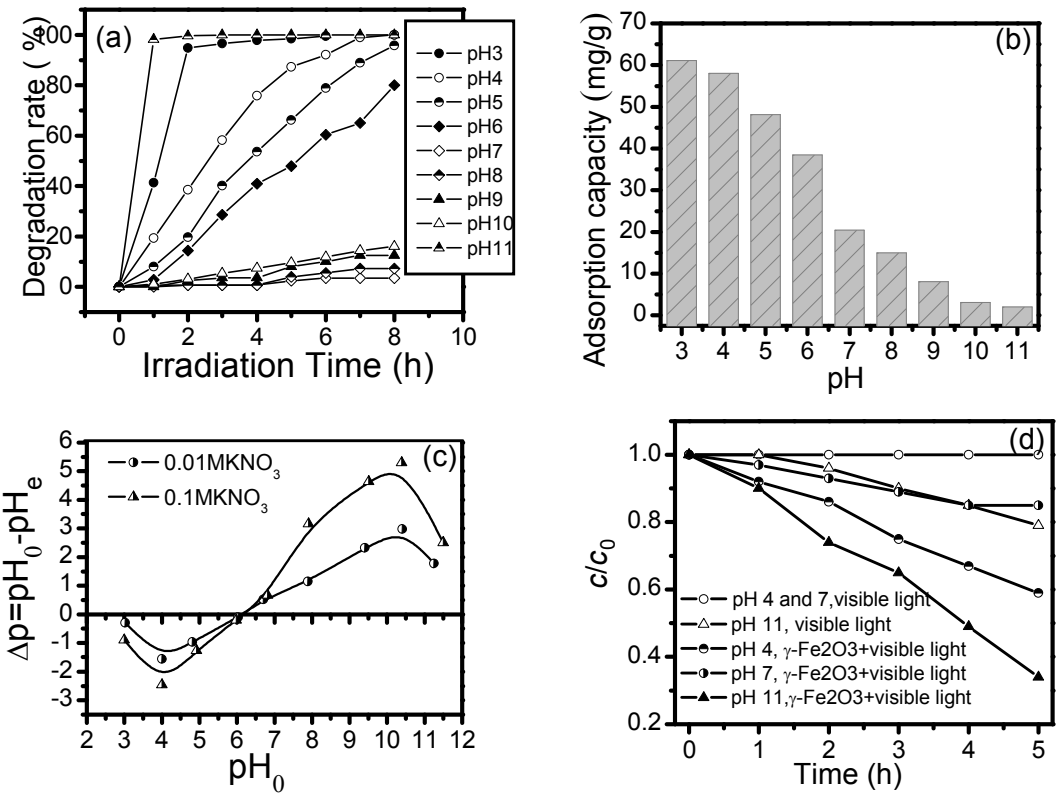

Fig. 7. (a) Changes of the degradation rate of AB 74 at different pHs with time.
(b) Changes of the adsorption capacity of AB 74 on γ-Fe_2O_3 with pH.
(c) The pH_{pzc} of γ-Fe_2O_3
(d) The catalytic decomposition of H_2O_2 at different pHs.

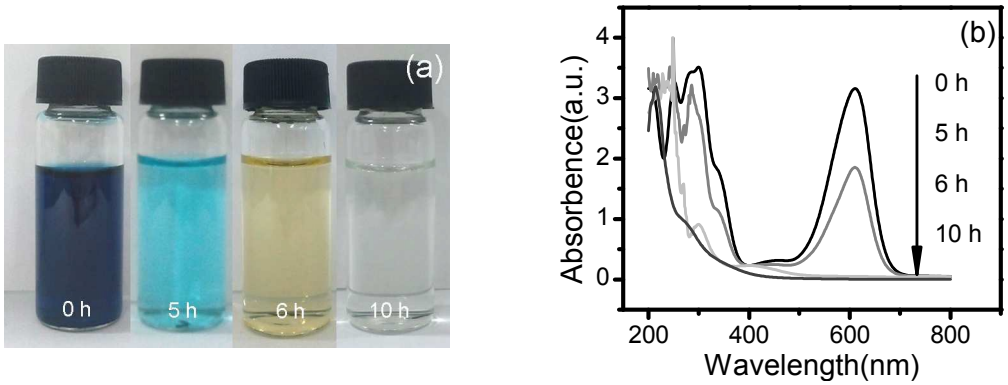

Fig. 8. Digital photos (a) and UV-vis absorption spectra (b) of the system at different times.

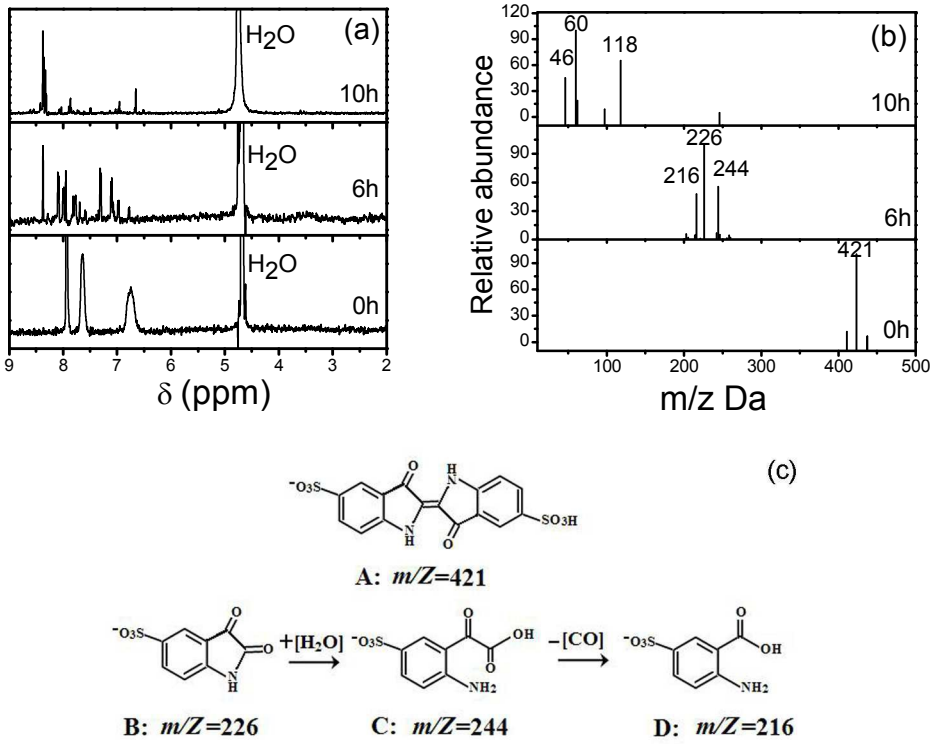

Fig. 9. (a) ^{1}H NMR spectra of AB 74 before irradiation and after 6 and 10 h treatment (solvent: D_2O). c_{AB74}=100 mg/L; c_{H2O2}=0.01 mol/L; natural pH; 5 ml treated.

(b) ESI(-)-MS of AB 74, samples withdrawn at 6 and 10 h.

(c) The degradation products of AB 74 in aqueous solution

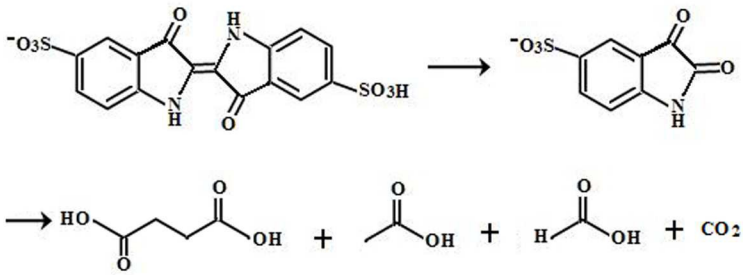

Fig. 10. Proposed mechanism for the degradation of AB 74 in the present system